DØnote 4333

# Dataset and topological analysis used in the $t\bar{t}$ production cross section analyses in the all-jets channel using p14 data

Freya Blekman, Marcel Vreeswijk

(Dated: March 22, 2004)

This note describes the basic analysis methods for the analyses done on the $t\bar{t}$ →all-jets production cross section measurement. We discuss the dataset, trigger requirements and basic topological variables which are used in the analyses using the different b-taggers: SVT (single tag) in DØ note 4346 and the soft muon tagger in DØ note 4347.

*Preliminary Results for Winter 2004 Conferences*

**Changes with respect to the p13 analysis**

The analysis that we present in this note is very similar to the analyses done in Run 1[2] and in Run 2 for the Lepton/Photon conference in 2003[1]. There are some differences, which are listed here.

- The efficiency to trigger top events is determined on data. We parametrize the trigger efficiency for the different trigger levels by multiplying with the efficiency as a function of the reconstructed jet and event energies. The trigger is discussed in section III.
- Skimming and selection is done centrally, through the DØ Common Samples Group. See section III through V. There are slight changes in the trigger and skimming criteria, but as these criteria are still quite loose, there is no significant influence on the final selection cut on jet multiplicity (equation 1).
- Different reconstruction and top_analyze versions are used. The versions are specified in section IV. One of the more major changes is the use new, noise reducing, calorimeter reclustering algorithms, which has an influence on the jet energy spectra. This has a direct consequence on the shape of energy-scale dependent topological variables, which are discussed in section VII B.
- The detector smearing of jets and muons in Monte Carlo is taken into account in our Monte Carlo samples.
- The use of the mass likelihood variable $\mathcal{M}$ has changed. We now have two separate $\chi^2$-like variables for the W-mass and t-mass information, respectively.
- The cut on $nn1 > 0.05$, which was used to reject background in the final $nn2$ distributions, has been removed from the analysis.

## I. INTRODUCTION

This note will describe the analysis method used to do the measurement of the $t\bar{t} \rightarrow$ all-jets production cross section with a dataset taken at the start of Run II, with $\sqrt{s} = 1.96$ GeV/c$^2$. First we will discuss the triggers and other dataset definitions (section III), after which we continue by discussing the analysis method using several artificial neural networks. Different types of $b$-jet identification can be used in combination with the topological analysis described in this note. The analysis presented here is very similar to the one conducted on data reconstructed with the *p13* reconstruction in the summer of 2003[1], which itself was based on the Run I analysis[2].

## II. ANALYSIS OUTLINE

As was also mentioned in previous DØ publications [2], event selection for hadronic $t\bar{t}$ production channels mainly consists of rejection of QCD multi-jet background. The QCD background is expected to mainly consist of hard scatter $2 \rightarrow 2$ parton processes with extra jets created through soft QCD interactions. Though more than half of the hadronic top events are expected to only have five or less reconstructed jets, the reduction in background makes it worthwhile to require six or more jets. The presence of six jets also makes it possible to calculate the four-momenta of all partons in the $t\bar{t}$ system, so we can reconstruct the masses of the t quarks and the $W$ bosons.

We do not correct muon-tagged jets for the difference in jet energy scale from the non-measured neutrino, as we use the same (assumed light quark) jet energy scale for all jets. The main reason for this is the fact that our background, for which we use untagged data events, is used to predict the background content in our distributions. This comparison becomes much more difficult when different jet energy scales are used for the tagged and untagged samples.

The analysis consists of the following steps:

1. Event selection.
   We separate our sample into two subsamples:

   I. Tagged Events:
   Events which contain a b-tag. These events are expected to have a much larger probability of being a top-event. These events are further referred to as our signal sample.

   II. Untagged Events:
   Events which contain no tag. This sample is dominated by QCD background. These events are used as our background sample.

2. First background reduction. ($NN0$)
   A simple artificial neural network is used for the first pre-selection on event kinematics and topology. This neural net is trained on the variables expected to have the most discriminating power. Events which have a $NN0$ discriminant smaller than 0.05 are discarded from the further analysis. The cut value of $NN0 > 0.05$ has not been optimized, as it was inherited from the Run 1 analysis. However, it does not significantly cut into our signal and removes background-like events from our analysis. On the sample that is left after this selection we determine the probability to tag a jet, using a tagging probability function we call a Tag Rate Function (TRF).

3. Neural Network 1. ($NN1$)
   After rejection of the obvious background, a first neural network is applied to provide one discriminating variable for all the (heavily correlated) event-shape variables. This $NN1$ uses the same input variables as $NN0$ and some extra topological variables, which are all discussed in section VII B.

4. Neural Network 2. ($NN2$)
   After the first neural net, the data are processed with a second neural network ($NN2$), that combines the output of $NN1$ with extra top quark properties. Here we also have the possibility to include b-tagging information.

Though the separate use of $NN1$ and $NN2$ causes us to lose the information that $NN1$ had on the correlations between the different variables, this method has the advantage that we can re-use the neural network in analyses using other $b$-identification methods. Also, in Run 1 it was shown that there were only very small correlations between the $NN1$ and $NN2$ variables.

## III. TRIGGER

We select events that fired the 4JT10 (trigger lists v8 through v11) or 4JT12 (v12 trigger lists) triggers, which consist of the following trigger terms

- 4JT10:

L1: CJT(4,5)

- Four trigger towers with $E_T > 5$ GeV.

L2: 3jet8_ht90

- Three jets above with $E_T > 8$ GeV and total $H_T > 90$ GeV. The $H_T$ cut is not made in trigger list v8.

L3: mp160_JET(SCJET_9,4,10.)_JET(SCJET_9,2,20.)

- Four jets with $E_T > 10$ GeV, of which two with $E_T > 20$ GeV. The JET(SCJET_9,2,20.) cut was not made in trigger list v8.

- 4JT12:

L1: CJT(3,5)

- Three trigger towers with $E_T > 5$ GeV.

L2: 3jet8_ht50

- Three jets with $E_T > 8$ GeV and total $H_T > 50$ GeV.

L3: mp160_JET(SCJET_9,4,12.)_JET(SCJET_9,3,15.)_JET(SCJET_9,2,25.)

- Four jets with $E_T > 12$ GeV, of which 3 with $E_T > 15$ GeV and two with $E_T > 25$ GeV.

### A. Trigger efficiency

The trigger efficiency was measured using the *top_trigger*[9] package. This package uses the jet-based trigger turn on curves to calculate the probability that the event was triggered. We use this probability as an event weight in our analysis. The different jet turn-ons are considered uncorrelated, and the calculations are done as described in [4].

We show the turn-on curves (Figures 1 through 4) for the different terms used in the three trigger levels. The efficiency was measured on the top group's **jettrig** skim, which is taken with a simple single electron trigger. We require the electron to have triggered the single electron trigger (by requiring that at least 10 GeV was already present at the second trigger level), and then look at the remaining jets. This method is also used in the other jet trigger studies done in the top group[3].

Note that, even though the description in the lower values of $p_T$ and $H_T$ is sometimes not perfect, the expected $t\bar{t}$ contribution is typically on the plateau.

The average efficiency for signal was measured to be:

$$\epsilon(N_{jets} \geq 6, nn0 > 0.05) = 0.77 \pm 0.004,$$

which is considered a conservative estimate. We derive this number from figure 5, which shows the efficiency of the whole trigger as a function of a neural network discriminant.

The efficiency before the neural network selection is obviously lower, but contains events which would not be selected in the final analysis.

This trigger efficiency corresponds within reasonable limits with the efficiencies determined from trigsim (table I) and data studies in p13 reconstruction releases (85-90%). A luminosity weighed average for the whole dataset would lead to an average of

$$\epsilon(t\bar{t}, \text{trigsim}) = 0.91.$$

We use the difference between the parametrized trigger efficiency and the efficiency from the trigger simulator into account as a systematic uncertainty on the final analysis. In the total signal efficiency calculation in the cross section analysis, the influence of the trigger efficiency is taken into account on an event-by-event basis.

| trigger versions and luminosity | | | |
|---|---|---|---|
| trigger list version | trigger | $\epsilon$(trigsim) | Integrated luminosity [$pb^{-1}$] |
| v8 | 4JT10 (no L2 $H_T$) | 95% | 20.8 |
| v9 | 4JT10 | 91% | 29.1 |
| v10 | 4JT10 | 91% | 15.8 |
| v11 | 4JT10 | 91% | 57.8 |
| v12 | 4JT12 | 91% | 38.9 |

TABLE I: *Luminosity and efficiency from the trigger simulator for different trigger versions. The v12 trigger list has the same efficiency as the v9-11, but the background rejection was moved from the second to third trigger level*

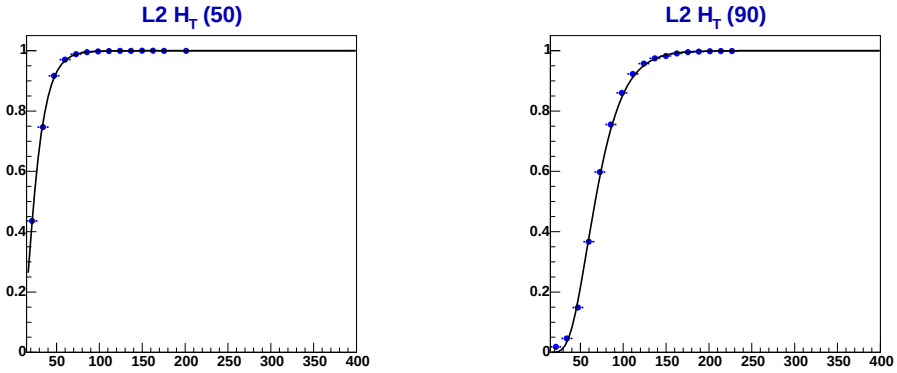


FIG. 1: *Trigger turn-on curves for L2 $H_T$ for the two different values of L2$H_T$¿50,90 GeV/$c^2$.*

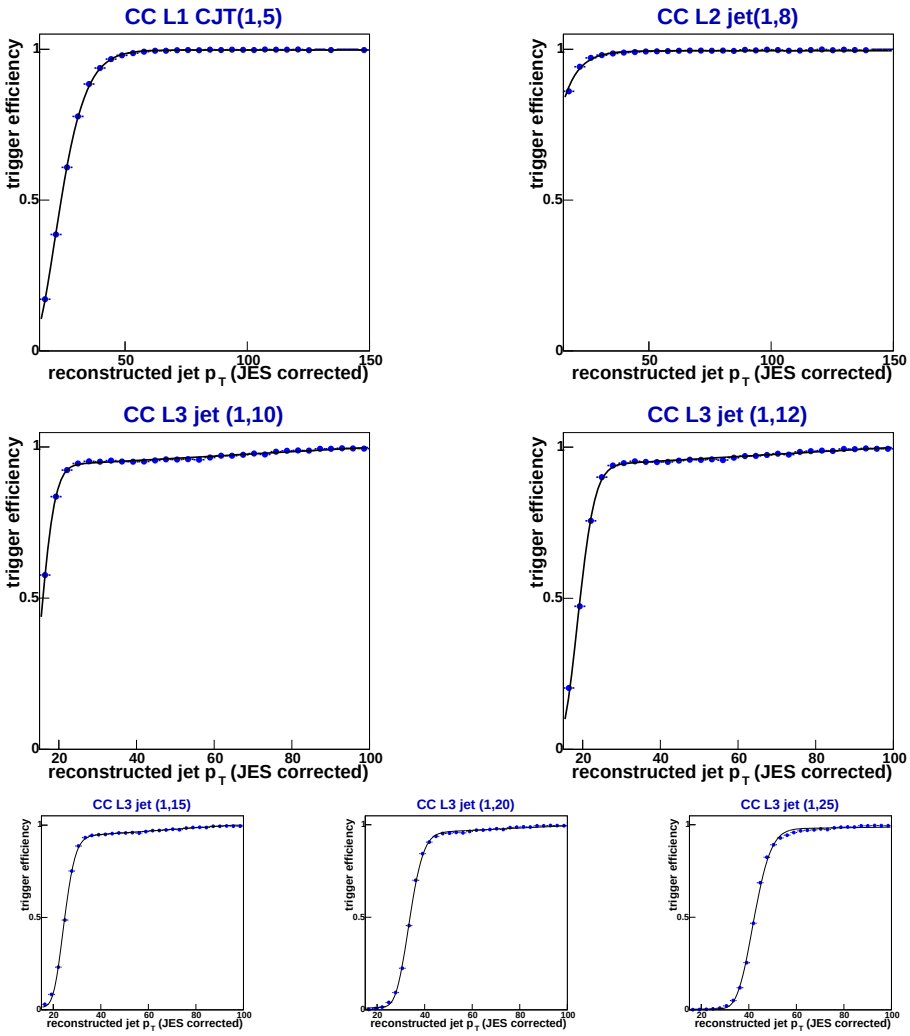


FIG. 2: *Trigger turn-on curves for jets in the Central Calorimeter* ($|\eta| < 0.8$).

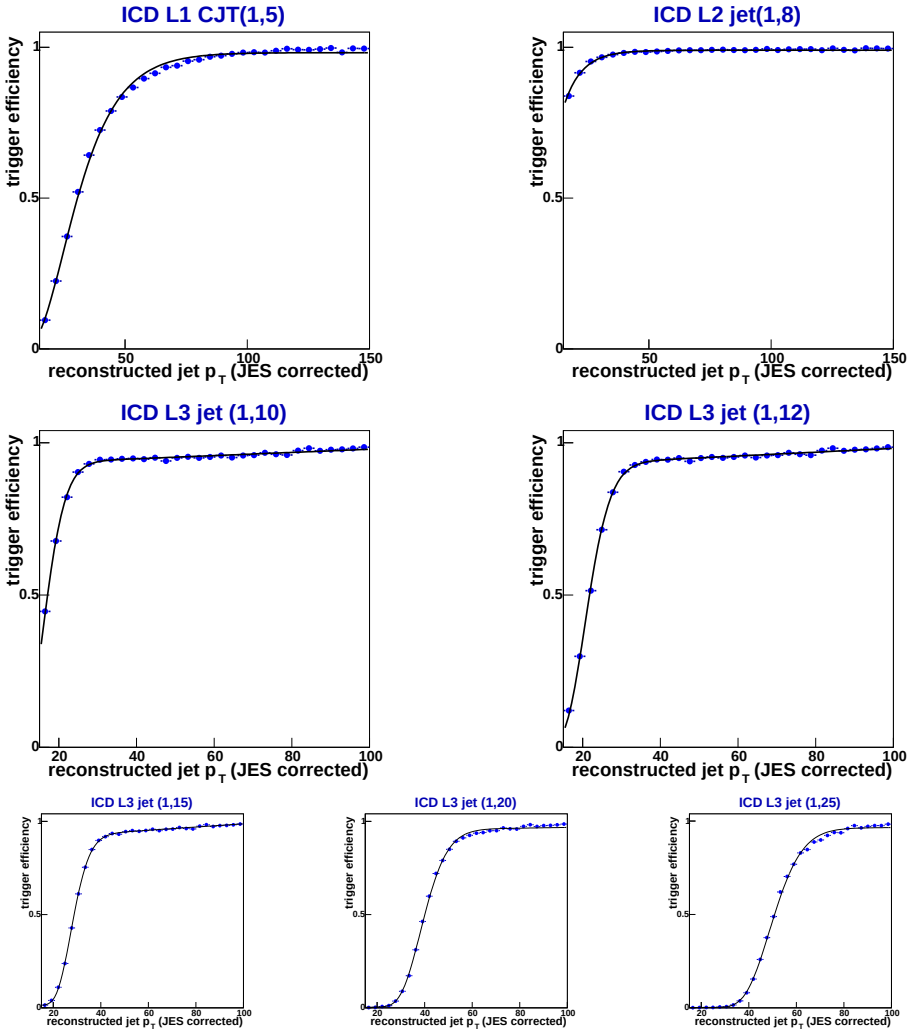


FIG. 3: *Trigger turn-on curves for jets in the Inter-Cryostat Detector Calorimeter* ($0.8 < |\eta| < 1.5$).

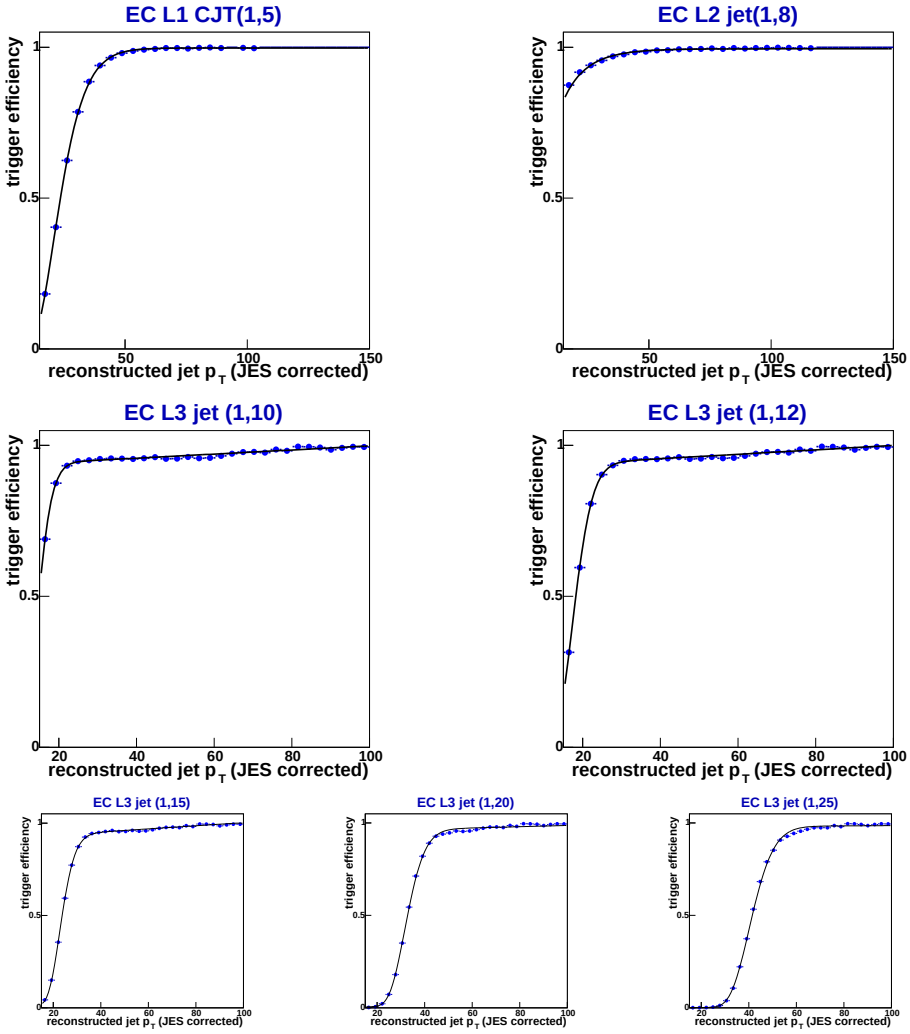


FIG. 4: *Trigger turn-on curves for jets in the Endcap Calorimeter* ($|\eta| > 1.5$).

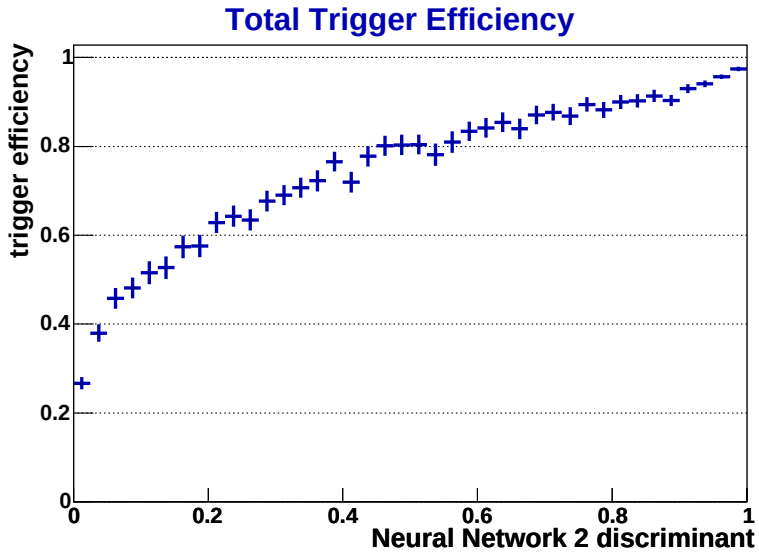


FIG. 5: *Complete trigger efficiency as a function of one of the analysis discriminant neural nets, NN2.*

## IV. DATA SAMPLES

Multi-jet data is collected and reconstructed using the common samples group's3JET skim[5]. This skim selects events with the following properties:

- Event passed a multijet trigger. The top triggers 4JT10 (v11 trigger lists and earlier) or 4JT12 (v12 trigger lists) are included in the used triggers. For definition of these triggers see section III.
- Events contain at least 3 reconstructed calorimeter jets, where there are no further jet quality cuts applied. We use 0.5 cone jets.

After this pre-selection, these events are processed and skimmed further with the **Nefertiti** version of *top_analyze* [6], using DØ production release **p14.05.01**. We then require the presence of at least 4 reconstructed jets. Here a set of quality requirements[5, 6] is already applied on the jets.

### A. Good Run Lists

After processing to root-tuple level, the dataset still contains data that was taken during periods when the various sub-detectors were not performing optimally.

The good run list used in this analysis is provided through the *top_dq*[8] package. Top_dq takes into account tracking, calorimeter and DAQ system performance on luminosity block basis. It also contains the option to have an extra rejection of runs in which the quality of the reconstructed muons is poor. The extra muon quality requirement will only be used in $t\bar{t} \rightarrow$all-jets analyses that use soft muons. After the data quality requirements, we are left with analysis sample of which the two signal triggers have been exposed to a total integrated luminosity of 162 pb$^{-1}$. When the additional muon quality requirements are applied, we are left with a sample of 150 pb$^{-1}$.

## V. MONTE CARLO SAMPLES

In this note, we use a sample of 47,500 $t\bar{t} \rightarrow \mathrm{all-jets}$ Monte Carlo events for signal simulation. This would be equivalent to a top sample collected with 100% efficiency at an integrated luminosity of approximately 160 fb$^{-1}$. We do not include hadronic $\tau$ decays in our sample if the $\tau$ lepton originates from the leptonically decaying $W$ bosons from the $t\bar{t}$ decay. To study the behavior of $t\bar{t} \rightarrow \tau$+jets we have an inclusive lepton+jets sample, which includes $t\bar{t} \rightarrow$any lepton+jets $W$ boson decays. This sample

The used events have been generated with the PYTHIA generator in the **mcp14** DØ Monte Carlo version. The exact definitions can be found on the top group's Monte Carlo pages[10]. A random number of underlying minimum bias events was added, using a Poisson distribution with a mean of 0.8. We use a top mass of $M_{top} = 175$ GeV/c$^2$, and use smaller samples with $M_{top} = 165, 185$ GeV/c$^2$ for systematic studies. All Monte Carlo is corrected for the smearing of $\mu$ and jet energy by the DØ detector. The simulated $t\bar{t}$ events were reconstructed with the same top_analyze version as the used dataset.

| Different pre-selection cuts | | |
|---|---|---|
| | $\epsilon(t\bar{t}$ MC) | $\epsilon$ for 6-jet data |
| isolated EM | 0.9993 | 0.9901±0.0001 |
| isolated $\mu$ | 1.0000 | 1.000±0.0000 |
| $N_{prim.Vtx} = 0$ | $1.0\text{-}7 \cdot 10^{-3}$ | 0.9902±0.0001 |
| $N_{jets} \leq 6$ | 0.438 | |
| In final analysis sample | | |
| $N_{jets} \leq 6$ | 0.438 | 292202 |

TABLE II: *Numbers of events rejected for different event quality cuts. Note that the jet multiplicity cut is made last in the preselection*

## VI. PRE-SELECTION

We require the event to have no isolated electron or muon, to provide an orthogonal dataset to the datasets used by the analyses of the other $t\bar{t}$ decay channels. The isolated lepton veto results in no signal efficiency reduction. The specific isolation criteria for leptons are as used in the $t\bar{t} \rightarrow l+$jets analyses. After the application of data quality requirements, we are left with the vetoes on isolated muons have no effect, and we find only 65 isolated electrons in events that also contain 6 or more calorimeter jets.

To be able to have a accurate description of the momenta of the different objects in the event, we require the presence of at least one primary vertex (PV), where we require that PV to be within 60 cm of the center of the detector, and have at least 3 tracks associated with it. This cut was measured to be over 99% efficient on data events with 6 or more jets.

We then apply the following pre-selection cut:

$$N_{jets} \geq 6 \tag{1}$$

Statistics for rejected events can be found in table II.

After preselection we are left with 292202 6-jet events, which corresponds to an integrated luminosity of 162 events/pb.

## VII. QUANTITIES USED FOR EVENT SELECTION

### A. Introduction

In this section we discuss the various kinematic variables we use in the kinematic $t\bar{t} \rightarrow$all-jets analysis. This analysis by itself does not have enough discriminative power to distinguish between signal and background, but one can apply b-identification afterwards to surpress background. In this note we only discuss the kinematic part of an analysis like this.

### B. Definition of kinematic variables

The variables used to distinguish hadronic top signal from QCD multi-jet background can be distinguished into five categories:

(i) Distinction between energy scale. QCD background tends to have an overall lower transverse energy distribution, jets are less energetic and the total invariant mass of the event is smaller than in $t\bar{t}$ events. Even though the average jet energy is smaller in QCD events, the leading jets tend to be more energetic in QCD than in $t\bar{t}$ events. The variables used here are $H_T$ and $\sqrt{s}$.

(ii) Soft non-leading jets. As the QCD background mainly consists of hard 2-jet processes with extra soft gluon jets, the additional jets are expected to be softer in QCD background than in $t\bar{t}$ signal. The variables we use are $H_T^{3j}$, $E_{T_{5,6}}$ and $N_{jets}^{A}$.

(iii) Event Shape. These quantities qualify the behavior of the angles and sizes of jets in the event as a whole. Top events have a different shape as QCD background. The jets are almost spherically distributed in top events, while QCD events usually have a more back-to-back jet distribution. We use *aplanarity* and *sphericity* to quantify this difference between signal and background.

(iv) Rapidity distribution. These quantities are used to identify where the set of jets in the event was observed in the detector. Because of their typical hard scatter origin, the jets in QCD background events are expected to be more back-to-back than top signal, while QCD events are also more likely to be boosted in the direction of the beam-line. This has as a consequence that not all the jets in the event are expected to be central. We use *centrality* and $< \eta^2 >$.

(v) Typical top properties. The second neural network ($NN2$) is trained on properties which are very typical for top event structure, like the presence of W-bosons and b-quarks. The variables used are the W and top mass likelyhoods $\mathcal{M}_{WW}$ and $\mathcal{M}_{t\bar{t}}$, the $P_T$ of the soft muon, and the minimal di-jet masses $M_{min}^{1,2}$ and $M_{min}^{3,4}$.

These variables will be discussed in detail in the following paragraphs, and are also shown in figures 6 through 17.

#### (i) Parameters Sensitive to Event Energy Scale

Parameters sensitive to the energy scale of the whole event are typically also sensitive to the top mass. For this study, all top masses are presumed to be of value $M_{top} = 175$ GeV.

1. $H_T$. This parameter is defined as the total transverse hadronic sum the event, or:

$$H_T = \sum_{jet=1}^{N_{jets}} E_T(jet) \tag{2}$$

2. $\sqrt{\hat{s}}$. The invariant mass of all the jets in the event.

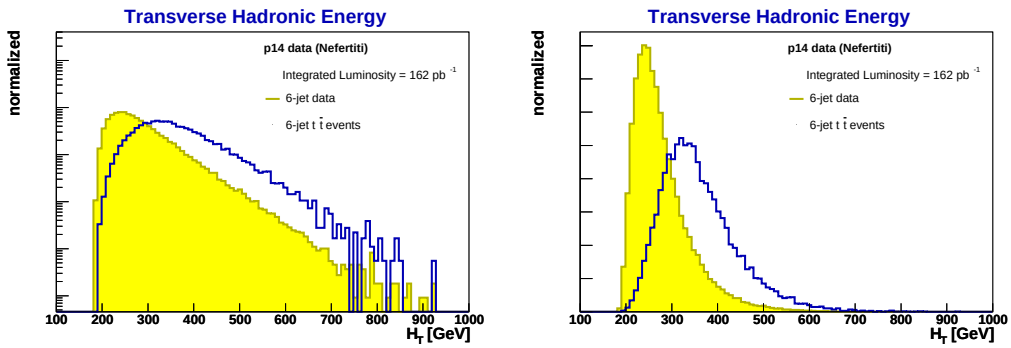


FIG. 6: *$H_T$ distribution for $t\bar{t}$ →all-jets Monte Carlo and 6-jet QCD data.*

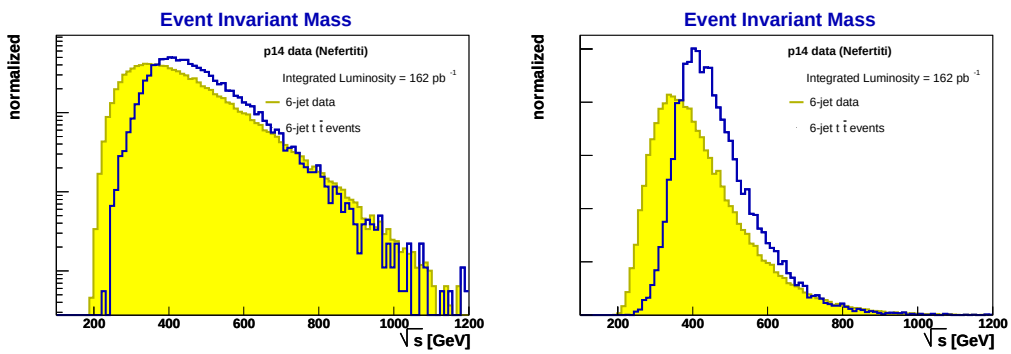


FIG. 7: *$\sqrt{s}$ distribution for $t\bar{t}$ →all-jets Monte Carlo and 6-jet QCD data.*

**(ii) Parameters Sensitive to Additional Radiation**

These variables are mainly used because they provide good distinction between hard $2 \rightarrow 2$ scatter processes with some extra soft jets and real multi-jet events.

3. $H_T^{3j}$. This variable is defined as [2]:

$$H_T^{3j} = H_T - E_T(\text{jet1}) - E_T(\text{jet2}), \tag{3}$$

where $E_T(\text{jet1})$ and $E_T(\text{jet2})$ are the leading and second-leading jet, respectively.

4. $E_{T_{5,6}}$ is defined as the geometric mean of the transverse energies of the fifth and sixth leading jet:

$$E_{T_{5,6}} = \sqrt{E_T(\text{jet5}) \cdot E_T(\text{jet6})} \tag{4}$$

5. $N_{jets}^A$ is the jet $E_T$ weighted average over the number of jets, which is defined as:

$$N_{jets}^A = \frac{\int_{15}^{55} E_T^{thr} N(E_T^{thr}) dE_T^{thr}}{\int_{15}^{55} E_T^{thr} dE_T^{thr}} \tag{5}$$

where $N(E_T^{thr})$ is the number of jets in a given event with $|\eta| < 2.5$ and $E_T$ greater than threshold value $E_T^{thr}$ [GeV]. This value is discussed in more detail in the Run I all-jets publication [2].

**(iii) Aplanarity and Sphericity**

Aplanarity and sphericity are defined as different combinations of the eigenvectors of the normalized momentum tensor. For more explanation see [2]. Here we mainly discuss the physical implications of the two variables.

7. *Sphericity* defines how spherical the jets in an event are. A perfectly spherical event has sphericity = 1. Top events are expected to be more spherical than QCD background events.

8. *Aplanarity* defines how the jets in the event are placed in respect to a plane. If the event system spans only one plane, the aplanarity is zero. An event is maximally aplanar when Aplanarity = 0.5. Top events tend to be more aplanar than QCD events

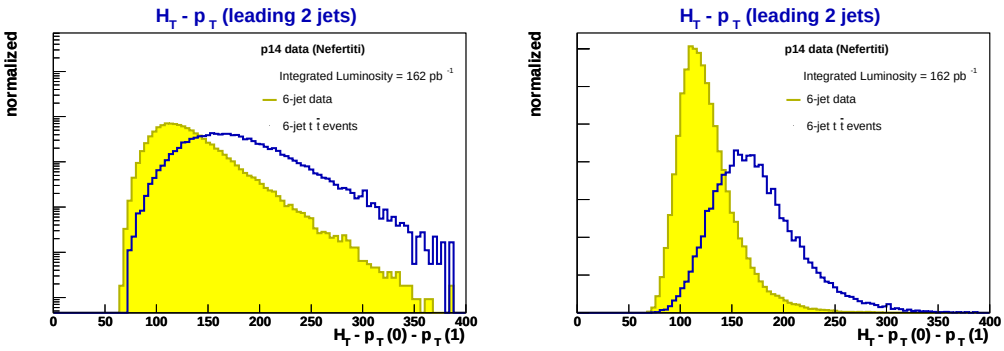


FIG. 8: $H_T^{3j}$ *distribution for* $t\bar{t}$ $\rightarrow$*all-jets Monte Carlo and 6-jet QCD data.*

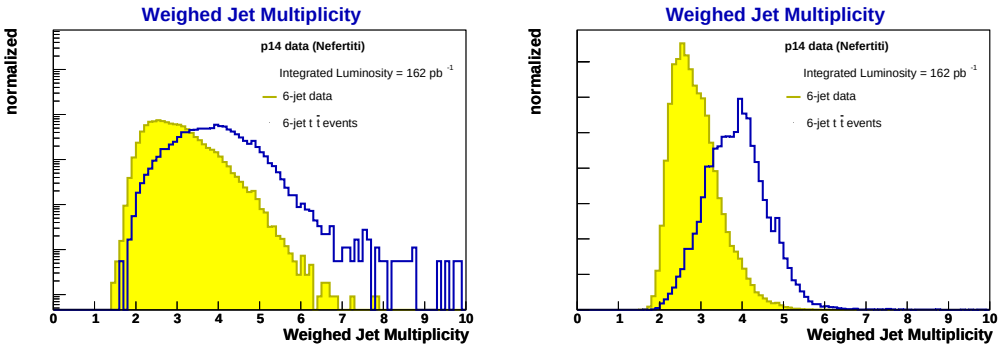


FIG. 9: $N_{jets}^{A}$ *distribution for* $t\bar{t}$ $\rightarrow$*all-jets Monte Carlo and 6-jet QCD data.*

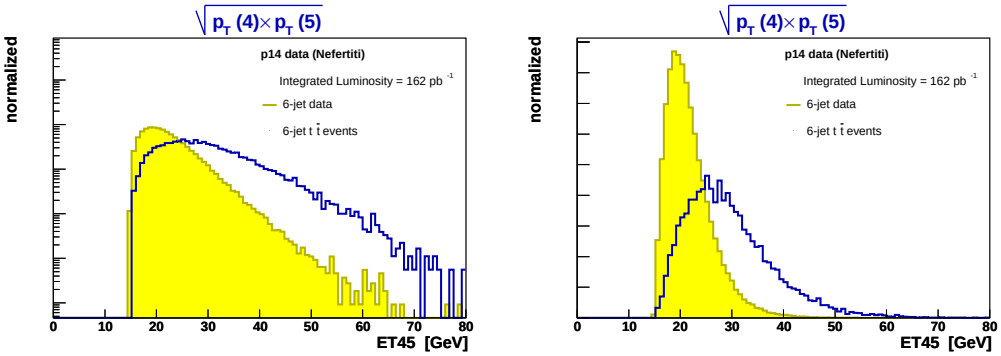


FIG. 10: $E_{T_{5,6}} = \sqrt{E_T(jet5) \cdot E_T(jet5)}$ *distribution for* $t\bar{t}$ $\rightarrow$*all-jets Monte Carlo and 6-jet QCD data.*

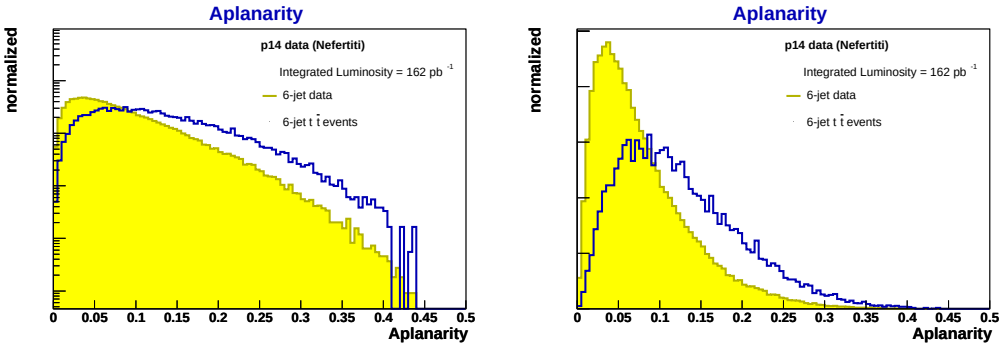


FIG. 11: *Aplanarity distribution for $t\bar{t}$ →all-jets Monte Carlo and 6-jet QCD data.*

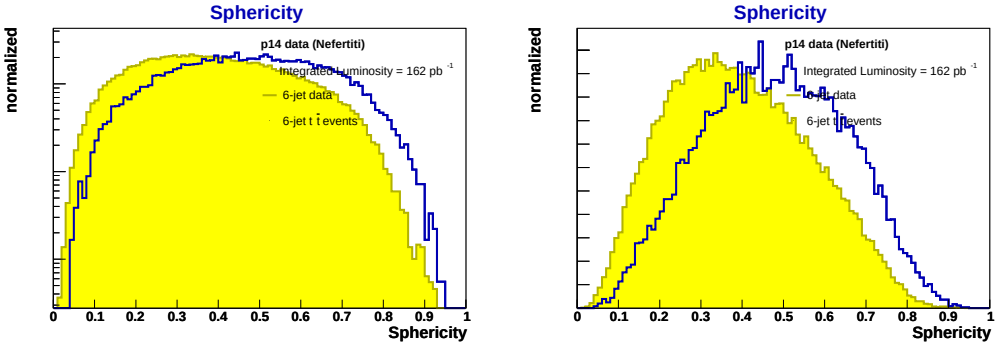


FIG. 12: *Sphericity distribution for $t\bar{t}$ →all-jets Monte Carlo and 6-jet QCD data.*

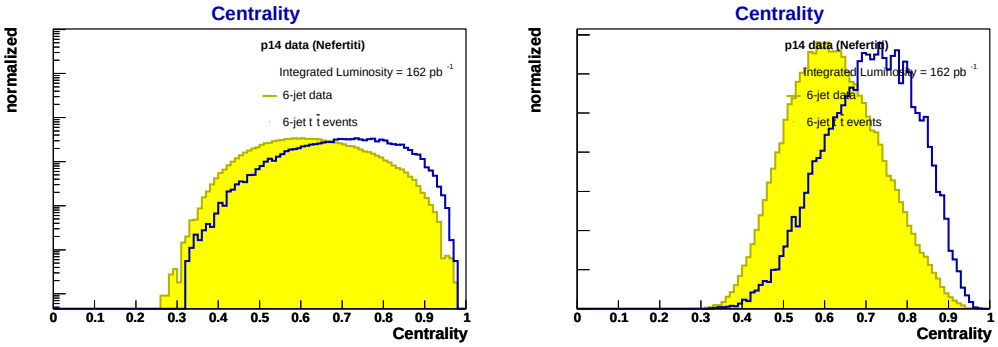


FIG. 13: *Centrality distribution for $t\bar{t}$ →all-jets Monte Carlo and 6-jet QCD data.*

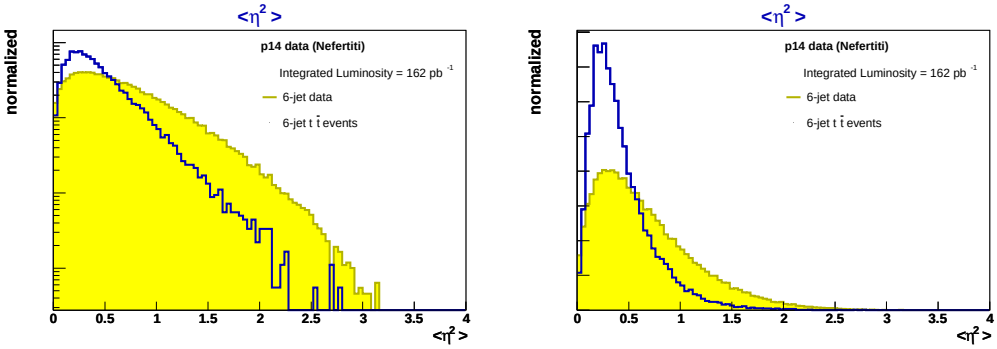


FIG. 14: $< \eta^2 >$ *distribution for $t\bar{t}$ →all-jets Monte Carlo and 6-jet QCD data.*

### (iv) Rapidity sensitive parameters

Top events are expected to have different pseudo-rapidity distributions than the QCD background, as they tend to be more central because of the higher transverse energy in the event. The following variables provide a handle on this quality:

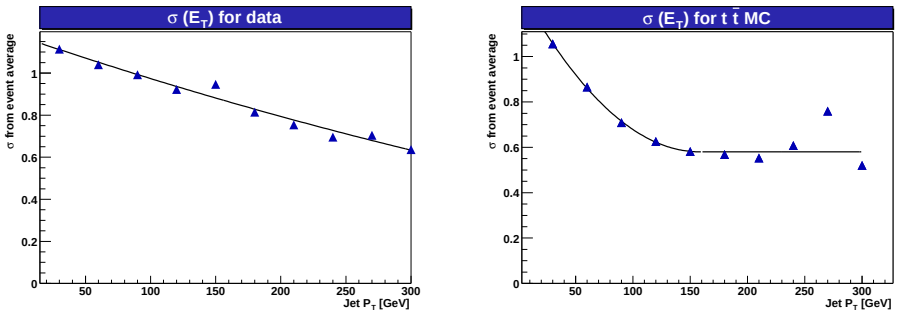


FIG. 15: *Distribution of $\sigma(E_T)$ for 6-jet events (triangles). Left plot gives the behavior for data, right plot for $t\bar{t}$ Monte Carlo. The solid lines are the fits that are used in equation (8).*

8. Centrality is defined as

$$\mathcal{C} = \frac{H_T}{H_E}, \tag{6}$$

where $H_E$ is the sum of all the jet energies in the event. The centrality provides a handle on what fraction of the energy deposited in the proton-antiproton collision is transverse energy.

9. $< \eta^2 >$ is the weighted RMS of the six leading jets in the event, and is defined by:

$$< \eta^2 > = \frac{\sum_{jet=1}^{6} \mathcal{W}(E_T)(\eta_{jet} - \bar{\eta})^2}{\sum_{jet=1}^{6} \mathcal{W}(E_T)} \tag{7}$$

where

$$\mathcal{W}(E_T) = \frac{\sigma^{t\bar{t}}(E_T) - \sigma^{background}(E_T)}{\sigma^{t\bar{t}}(E_T)} \tag{8}$$

and

$$\bar{\eta} = \frac{1}{H_T} \sum_{jet=1}^{N_{jets}} E_{T_{jet}} \eta_{jet} \tag{9}$$

The quantities $\sigma^{t\bar{t}}(E_T)$ and $\sigma^{background}(E_T)$ are the widths of the $\eta$ variance on jet basis, as a function of the jet $E_T$. $\sigma^{t\bar{t}}(E_T)$ and $\sigma^{background}(E_T)$ are the observed $\sigma$ of the jet distribution with respect to the center of the detector ($\eta = 0$), as a function of jet $p_T$. These distributions were measured in the p13 analysis [1], and the then measured values are still used in this analysis.

**(v) Other variables**

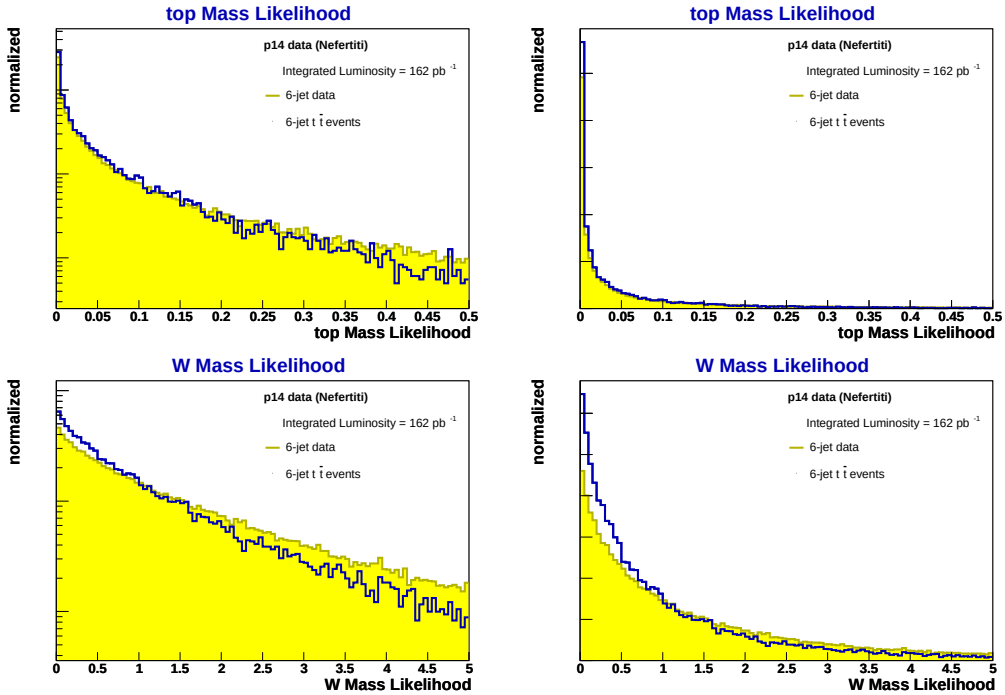


FIG. 16: *Distribution of the mass likelihood variables $\mathcal{M}_{t\bar{t}}$ and $\mathcal{M}_{WW}$ for 6-jet muon data (open histogram) and singal Monte Carlo (filled histogram).*

As was mentioned before, we also use variables which are not based on the event topology:

9, 10. The top and W mass likelihood of the event, $\mathcal{M}_{t\bar{t}}$ and $\mathcal{M}_{WW}$ ,which are $\chi^2$-like variables defined as:

$$\mathcal{M}_{t\bar{t}} = \frac{(m_{top_1} - m_{top_2})^2}{\sigma_{top}^2} \tag{10}$$

$$\mathcal{M}_{WW} = \frac{(M_{W_1} - M_W)^2}{\sigma_W^2} + \frac{(M_{W_2} - M_W)^2}{\sigma_W^2} \tag{11}$$

The widths $\sigma_{top}$ and $\sigma_W$ and W boson mass $M_W$ are obtained from $t\bar{t} \rightarrow hadrons$ PYTHIA Monte Carlo distributions, and have values $\sigma_{top} = 45\ GeV$ ,$\sigma_W = 10\ GeV$ and $M_W = 80\ GeV$. These are similar to the values used in the run 1 analysis.

To obtain these values, cone 0.5 reconstructed jets were used, and no actual parton-level jet matching was done. We also did not apply any $b$-jet identification to reduce combinatorics.

In previous analyses these two $\chi^2$s were added to have a single top-$W$ hypothesis check, but figure 16 shows that the difference in size between $\mathcal{M}_{WW}$ and $\mathcal{M}_{t\bar{t}}$ is about one order of magnitude, which would mean that there was only tested on the

presence of two $W$ bosons. As $\mathcal{M}_{t\bar{t}}$ has typically more discriminating power as $\mathcal{M}_{WW}$, making the distinction between the two quantities improves the analysis sensitivity.

13, 14. The smallest jet masses in the event. As all jets in top events are associated with high-mass objects, both the smallest di-jet mass $M_{min}^{1,2}$ and the second smallest di-jet mass $M_{min}^{1,2}$ can be a useful input variable. When calculating $M_{min}^{3,4}$, jets that were already used for $M_{min}^{1,2}$ are ignored. $M_{min}^{1,2}$ and $M_{min}^{3,4}$ are expected to be a smaller for QCD than for top events.

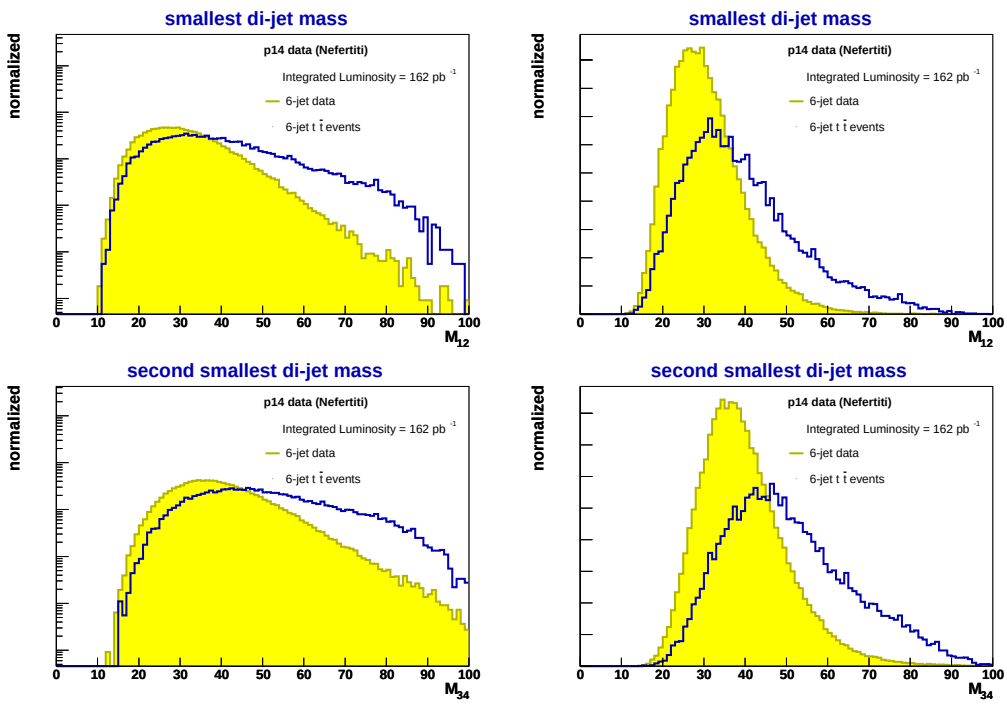


FIG. 17: *Distribution of the two minimal di-jet mass variables $M_{min}^{1,2}$ and $M_{min}^{3,4}$ for Monte Carlo (filled histogram), muon tagged events(markers) and predicted background(open histogram).*

## VIII. CORRELATIONS BETWEEN THE TOPOLOGICAL VARIABLES

The 13 parameters used in this analysis are correlated. To qualify the dependence between the variables we calculate the correlation, which is defined as:

$$r = \frac{\bar{xy} - \bar{x}\bar{y}}{\sigma_x \sigma_y} = \frac{\frac{1}{N}\sum x_i y_i - \frac{1}{N}\sum x_i \frac{1}{N}\sum y_i}{\sqrt{\frac{1}{N}\sum x_i^2 - (\frac{1}{N}\sum x_i)^2} \cdot \sqrt{\frac{1}{N}\sum y_i^2 - (\frac{1}{N}\sum y_i)^2}}.$$

The results of this correlation study are listed in table IV.

| | $H_T$ | $\sqrt{s}$ | $H_T^{3j}$ | $N_{jets}^A$ | $E_{T_{5,6}}$ | *Aplan* | *Spher* | *Cent* | $<\eta^2>$ | $M_{t\bar{t}}$ | $M_W$ | $M_{12}^{min}$ | $M_{34}^{min}$ |
|---|---|---|---|---|---|---|---|---|---|---|---|---|---|
| $H_T$ | 1 | 0.63 | 0.74 | 0.84 | 0.49 | -0.04 | 0.08 | 0.23 | -0.04 | 0.10 | 0.11 | 0.34 | 0.42 |
| $\sqrt{s}$ | | 1 | 0.52 | 0.56 | 0.35 | -0.40 | -0.42 | -0.45 | 0.33 | 0.19 | 0.27 | 0.31 | 0.40 |
| $H_T^{3j}$ | | | 1 | 0.79 | 0.77 | 0.13 | 0.10 | 0.12 | 0.02 | -0.00 | 0.03 | 0.37 | 0.41 |
| $N_{jets}^A$ | | | | 1 | 0.57 | 0.03 | 0.10 | 0.19 | -0.02 | -0.01 | 0.06 | 0.43 | 0.51 |
| $E_{T_{5,6}}$ | | | | | 1 | 0.12 | 0.07 | 0.07 | 0.03 | -0.02 | 0.03 | 0.42 | 0.43 |
| *Aplan* | | | | | | 1 | 0.69 | 0.58 | -0.27 | -0.12 | -0.15 | 0.03 | 0.01 |
| *Spher* | | | | | | | 1 | 0.74 | -0.38 | -0.12 | -0.19 | 0.03 | 0.02 |
| *Cent* | | | | | | | | 1 | -0.37 | -0.09 | -0.16 | -0.02 | -0.05 |
| $<\eta^2>$ | | | | | | | | | 1 | 0.08 | 0.14 | 0.01 | 0.02 |
| $M_{t\bar{t}}$ | | | | | | | | | | 1 | 0.20 | -0.06 | -0.07 |
| $M_W$ | | | | | | | | | | | 1 | 0.00 | 0.01 |
| $M_{12}^{min}$ | | | | | | | | | | | | 1 | 0.71 |
| $M_{34}^{min}$ | | | | | | | | | | | | | 1 |

TABLE III: *Average correlations among the 13 parameters for 6-jet data events*

| | $H_T$ | $\sqrt{s}$ | $H_T^{3j}$ | $N_{jets}^A$ | $E_{T_{5,6}}$ | *Aplan* | *Spher* | *Cent* | $<\eta^2>$ | $M_{t\bar{t}}$ | $M_W$ | $M_{12}^{min}$ | $M_{34}^{min}$ |
|---|---|---|---|---|---|---|---|---|---|---|---|---|---|
| $H_T$ | 1 | 0.80 | 0.74 | 0.65 | 0.44 | -0.11 | -0.15 | 0.35 | -0.18 | 0.28 | 0.11 | 0.34 | 0.39 |
| $\sqrt{s}$ | | 1 | 0.64 | 0.54 | 0.39 | -0.28 | -0.37 | -0.12 | 0.36 | 0.35 | 0.19 | 0.33 | 0.40 |
| $H_T^{3j}$ | | | 1 | 0.88 | 0.73 | 0.15 | 0.06 | 0.20 | -0.03 | 0.23 | 0.05 | 0.40 | 0.41 |
| $N_{jets}^A$ | | | | 1 | 0.77 | 0.18 | 0.10 | 0.22 | -0.04 | 0.16 | 0.03 | 0.49 | 0.51 |
| $E_{T_{5,6}}$ | | | | | 1 | 0.16 | 0.07 | 0.11 | 0.07 | 0.14 | 0.01 | 0.49 | 0.47 |
| *Aplan* | | | | | | 1 | 0.69 | 0.31 | -0.35 | -0.07 | -0.09 | 0.07 | 0.06 |
| *Spher* | | | | | | | 1 | 0.38 | -0.48 | -0.05 | -0.10 | 0.01 | -0.00 |
| *Cent* | | | | | | | | 1 | -0.65 | -0.04 | -0.05 | 0.04 | 0.04 |
| $<\eta^2>$ | | | | | | | | | 1 | 0.08 | 0.09 | 0.02 | 0.03 |
| $M_{t\bar{t}}$ | | | | | | | | | | 1 | 0.05 | 0.09 | 0.12 |
| $M_W$ | | | | | | | | | | | 1 | 0.00 | 0.00 |
| $M_{12}^{min}$ | | | | | | | | | | | | 1 | 0.79 |
| $M_{34}^{min}$ | | | | | | | | | | | | | 1 |

TABLE IV: *Average correlations among the 13 parameters for signal Monte Carlo*

## IX. CONCLUSION

In this note we have discussed the dataset, triggers, preselection and topological and kinematic analysis needed to measure the $t\bar{t} \rightarrow$ all jets cross section. We will discuss b-tagging in other notes, as there is the possibility to conduct the analysis using different methods of $b$-quark identification.

[1] *F. Blekman and M. Vreeswijk*, **Measurement of the** $t\bar{t} \rightarrow$ hadrons **production cross section using p13 data** , DØ note 4175, July 2003.

[2] *DØ Collaboration*, **Measurement of the top quark pair production cross section in** $p\bar{p}$ **collisions using multijet final states**, Phys. Rev. D 60, 012001 (1999).

[3] *The Top Physics Working Group of the DØ Collaboration*, **DØ Top Analysis and Data Sample for the Winter Conferences 2004**, DØ note XXXX, http://www-d0.fnal.gov/Run2Physics/top/private/winter04/winter04_top_note_v0_3.ps

[4] *R. Schwienhorst* **Top Trigger Selection and Application of Turn On Curves to the Monte Carlo**, http://www-d0.fnal.gov/Run2Physics/top/d0_private/wg/triggers/Note_Reinhard_Jan2004.pdf, January 2004.

[5] **DØ Common Samples Group**, http://www-d0.fnal.gov/Run2Physics/cs/index.html

[6] *M. Klute, L. Phaf and D. Whiteson*, **TopAnalyze - A Framework Analyze Package for Top Group Analyses**, DØ note 4122, March 2003. More updated documentation at: http://www-d0.fnal.gov/ Run2Physics/top/d0_private/wg/top_analyze/ top_analyze_documentation.html

[7] *Jean-Roch Vlimant, Ursula Bassler, Gregorio Bernardi, Sophie Trincaz-Duvoid*, **Technical description of the T42 algorithm for the calorimeter noise suppression** DØ note 4146, December 2003.

[8] *G. Watts*, **top_dq**, data quality package of top group

[9] *B. Vachon*, **top_trigger**, trigger efficiency package of top group

[10] *P. Perea, A. Heinson and M. Zielinski*, **mcp14/mcp13 Event Samples**, http://www-d0.fnal.gov/Run2Physics/top/d0_private/wg/mc/p14.html